CONF-930830--4

WSRC-MS-92-388

FLOW INSTABILITY AND FLOW REVERSAL IN HEATED ANNULAR MULTICHANNELS WITH INITIAL DOWNWARD FLOW (U)

by H. N. Guerrero

Westinghouse Savannah River Company
Savannah River Site
Aiken, South Carolina 29808

Other Authors:

C. M. Hart
(WSRC)

A paper proposed for Presentation/Publication
at/in the 1993 National Heat Transfer Conference
Atlanta, GA
08/08-11/93

DISCLAIMER

FLOW INSTABILITY AND FLOW REVERSAL IN HEATED ANNULAR MULTICHANNELS WITH INITIAL DOWNWARD FLOW

(Submitted to the 1993 National Heat Transfer Conference
Session on Two Phase Flow and Heat Transfer in Multichannels.)

by H. N. Guerrero
and C. M. Hart
Westinghouse Savannah River Company

ABSTRACT

Experimental and theoretical results are presented regarding the stability of initial downward flow of single phase water in parallel annular channels of the Savannah River Site (SRS) fuel assembly. The test was performed on an electrically heated prototypic mockup of a Mark-22 fuel assembly. The test conditions consisted of mass fluxes, from 98 - 294 kg/m^2-sec, and inlet water temperatures of 25°C and 40°C. With increased power to the heaters, flow instability was detected, characterized by flow fluctuations and flow redistribution among subchannels of the outer flow channel. With increased power, a condition was observed indicating local subchannel flow reversals where certain subchannel fluid temperatures were high at the inlet and low at the exit. With additional power increases, a critical heat flux condition was reached in the outer channel.

The power to reach the first flow instability varied from 20% - 52% of the power required to reach fluid saturation at the assembly exit; consequently, fluid and heater wall temperatures were all below saturation. The power to reach critical heat flux was 64% - 77% of the saturation power, a significant increase over the power necessary to reach initial flow instability. A marginal stability analysis was performed which correlated well with the conditions leading to the initial flow instability.

INTRODUCTION

Because core flow is downward in the SRS K-Reactor, flow instability is possible in the event of a sudden flow decrease (e.g., following a loss-of-coolant or loss-of-pumping accident). The SRS fuel assemblies consist of parallel annular flow channels connected at both ends. Under the effect of residual reactor power, the bouyancy force is in a direction which destabilizes the flow, possibly resulting in flow oscillations and local flow reversals.

Previous studies regarding flow instability in the SRS fuel assemblies have concentrated on obtaining experimental data at high flow rates (1). Such studies are based on an inlet pipe break accident where a mismatch occurs between the relatively high residual reactor power and the cooling available from the decreasing flow. The mode of instability is the Ledinegg type; consequently, the previous studies have concentrated on obtaining the minimum of the system pressure drop vs. flow characteristic curve under various heat flux conditions.

The converse situation of low power and low flows, which is related to the loss-of-pumping accident, was studied briefly and it was found that the mechanism for flow instability may be different than that at high flows. Data of a similar nature appears in the literature for natural circulation flows in boilers, thermosyphons, and solar heaters. However, the flows in these studies are generally laminar, whereas the flows in the SRS fuel assembly are in the transitional Reynolds number range. These free convection loops are usually single loops (2). Natural convection flows in parallel channels have also been studied (3). A distinction of the SRS fuel assembly is that the channels have different heat inputs and the heaters forming the channels can transfer heat to either or both of two adjacent channels; and, there is a through flow while only natural convection flows are discussed in the mentioned references (2-4). Because there is insufficient data applicable to the reactor, a test program was conducted which utilized a full scale mockup with prototypic thermal and hydraulic response.

TEST OBJECTIVES

The objectives of this study were:

1) To establish a safety margin between the operating limit criteria of no boiling in the core, and a catastrophic thermal excursion resulting from a dryout conditionin the fuel assembly.

2) To provide the initial power to reach a flow instability and clarify the mechanism leading to initial boiling in the core.

TEST APPARATUS

The full scale mockup assembly (Figures 1 and 2a) comprises an outer target tube, outer heater, inner heater, and inner target; these heaters represent the fuel tubes in the fuel assembly. The outer, middle, and inner flow channels had pitch diameters of 85.6 mm, 66.6 mm, and 45.5, respectively, while the channel depths were 4.3 mm, 6.85 mm, and 5.1 mm. The rib gaps were 0.76 mm, with a tolerance of ±0.18 mm. The construction of the prototypic heaters (Figure 2b) consists of an inner aluminum tube, which held stainless-steel-sheathed, MgO-insulated, heating wires embedded in helical grooves. The pitch of the helical grooves varied continuously along the length of the tube which produced a chopped cosine heat flux distribution that peaked towards the bottom, with a peak-to-average ratio of 1.5. An outer layer of plasma-sprayed aluminum was deposited over the inner tube assembly, and then machined to final outside dimensions. The resulting heater was a monolithic structure with good thermal bonding between layers. For the inner heater, aluminum ribs were electron-beam welded to the outer surface. The heaters were instrumented with embedded thermcouples distributed at seven elevations and four subchannels. The outer and inner channels were instrumented with fluid thermocouples installed opposite the heater thermocouples and with pressure tap instrumentation in the four subchannel and at four elevations (Figure 1). Extensive testing showed that the heaters had similar thermal-

hydraulic performance to the fuel, and that the single phase channel flow distribution in the mockup was nearly equal to the known flow distribution of the fuel assembly.

In the test loop (Figure 1), demineralized water was pumped to a simulated section of the reactor plenum and flowed downward through the assembly mockup. At the exit of the mockup, the water entered a simulated reactor tank vessel and then flowed up a standpipe with an overflow height of 127 mm above the top of the plenum. This overflow height set the tank bottom pressure relative to atmospheric pressure. The water then flowed downward to the catch tank, from which it was pumped through a heat exchanger and back to the plenum.

Power to the theaters was provided by two banks of a silicon-controlled rectifier DC power supply and was independently controlled at a 60%/40%, outer to inner heater power split. Heater power inputs were measured with RMS voltmeter and RMS (Hall effect type) current transducers to eliminate errors caused from a small ripple at 360 Hz in the power supply output.

TEST PROCEDURE

The first step was to set the water flow and apply power to the heaters necessary to reach the desired loop water temperature by adjusting the heat exchanger cooling flow. When the desired inlet water temperature to the mockup was reached, the power was increased in increments of approximately 10 to 20% of the power to reach fluid saturation at the exit, while maintaining loop heat balance. When a thermal balance was achieved (indicated when the electrical power input to the heaters agreed with the heat absorbed by the fluid calculated from the mass flow and temperature increase of the fluid), a stabilization period of five to ten minutes was further maintained, steady state data for 5 minutes was collected, and power was increased to the next step. Data was recorded at the following power levels:

- When the fluid temperatures first began to fluctuate, indicating initial flow instability.

- When flow reversals became evident.
- When any of the fluid thermocouples reached saturation temperature.
- At the critical power for a thermal excursion.

The criteria for determining if a thermal excursion had occurred was for the wall temperature to increase rapidly at a rate similar to an adiabatic heatup rate which is indicative of a dryout condition. When the temperature exceeded 200°±25°C, the power was quickly reduced, terminating the test run.

TEST CONDITIONS

The conditions of the steady state tests were chosen where the system code, RELAP5, predicted the core flows to be minimum following a loss-of-pumping accident. The test conditions ranged from 0.31 to 0.94 kg/sec, total assembly flow rate; and inlet water temperature, 25°C and 40°C. The range in water flow rate covers the minimum assembly flow (0.62 kg/sec) and values above and below. The corresponding average mass fluxes (total flow divided by total flow area) were 98 to 294 kg/sec-m^2.

RESULTS

The following are results for a typical test run of 294 kg/sec-m^2 flow and 25°C inlet water temperature: At low powers, the fluid and heater wall temperature were uniform in all subchannels as illustrated in Figure 3a. The flow is considered as stable; as power increased, the stable condition changed at a specific power (183.2 kw), which was repeatable, when the fluid temperatures started to fluctuate with peak-to-peak amplitudes greater than 5°C and a period of 1-2 minutes (Figure 4); the time-averaged temperature profiles (Figure 3b) indicated that a flow redistribution occurred between the four subchannels of the outer channel; uniform flow was maintained in the middle and inner channels; when power was again increased to 197 kw, a trend to a flow reversal was observed in one or more subchannels in the outer channel (Figure 3c). This flow re-

versal is inferred from the increase in fluid temperature from bottom to the top of the subchannel D (where some mixing with the incoming cold water may have occurred), opposite to the trends of the other subchannels (which agree with expectations for downflow inside the subchannels). It is also at this power where the heater wall temperature first reached the fluid saturation temperatuere at the maximum heat flux location (Twall=Tsat). The local flow reversal did not initiate a catastrophic dryout on the surface of the outer heater because the heat could still be transferred to the adjoining middle channel; consequently, the heater power could be increased further under stable conditions. A higher power (227 kw) was then reached when all the subchannels in the outer channel uniformly exhibited an increasing temperature from bottom to top of the channel (Figure 3d). It was also at this power that a flow reversal occurred in the middle channel (concluded from the higher temperatures at the inlet of the middle channel compared to the outlet). Finally, a critical power (231 kw) was reached and a dryout condition occurred on the surface of the outer heater, resulting in a thermal excursion. In terms of the R-factor (defined as the ratio of the assembly power to the power required to reach bulk saturation conditions at the channel exit), the initial flow instability was reached at R=0.53, initial flow reversal and initiation of boiling at R=0.55, and thermal excursion at R=0.69.

The same general trends were repeated for other test runs at other flows and inlet water temperature. In all tests other than the above test case, no flow reversal was observed in the middle channel at lower powers than the thermal excursion power. When a uniform upward flow was reached in the outer channel, a thermal excursion immediately ensued.

The data is summarized in Table 1. The listed flows are accurate to ±1%, inlet temperatures to ±0.3°C, and powers to ±1.8% (2 σ limits). Figures 4 and 5 plot the data for two inlet water temperature cases, 25°C and 40°C. The lowest dotted lines delineate the stable (below the line) and unstable regions. For the highest flow (294 kg/sec-m^2), the power to reach Twall=Tsat appear to be equal to the power to reach initial flow reversal. The increments in power however

were not sufficiently small to resolve the question of which event preceded the other. It is clear though that at the two lower flows (98 and 196 kg/sec-m^2) flow reversal occurs well below the power to reach fluid saturation at the heater wall. Therefore, flow reversal causes boiling and not the other way around, which is the case for flow instability at very high flows. The points where thermal excursions were reached are plotted with a solid line. From Figures 4 and 5, assembly powers leading to the above phenomena appear to vary linearly with flow. There is also a large margin between the point of initial flow instability and the thermal excursion point of 26% of the power to reach initial instability at 294 kg/sec-m^2 and much larger at low flows.

FLOW INSTABILITY ANALYSIS

The following one dimensional analysis proposes a mechanism leading to the first flow instability : Consider a system of parallel channels with common inlet and outlet plena. The pressure drop across any channel is constant and equal to the system pressure drop despite changes in flow in such channel.

$$\Delta Pi = \Delta Pn \, . \qquad [1]$$

Assuming fluid properties are constant except for density in the bouyancy term, continuity implies velocity is constant in the channel and is a function of time only:

$$\hat{u} = \hat{u}(t) \, . \qquad [2]$$

The fluid density is approximated by

$$\rho = \rho_1[1 - \beta(\hat{T} - T_1)] \, , \qquad [3]$$

and the fluid viscosity by

$$\nu = \nu_0[1 - \alpha(\hat{T} - T_1). \qquad [4]$$

The momentum equation integrated over the length of a channel is given by

$$L\frac{d\hat{u}}{d\hat{t}} + \frac{\Delta P}{\rho_1} + \frac{fL\hat{u}^2}{2D} - \int g\,[1 - \beta(\hat{T} - T_1)]d\hat{s} = 0 \, . \qquad [5]$$

A single expression for the friction factor covering both laminar and turbulent flow ranges (350 <Re<6500) in the experiment was obtained from a curve fit of pressure drop data,

$$f = a_0 + \frac{a_1}{Re} + \frac{a_2}{Re^2} \, , \qquad [6]$$

where a_0 =0.01433, a_1=78.05 and a_2=4706.

The momentum equation then becomes,

$$\frac{d\hat{u}}{d\hat{t}} + [a_o + \frac{a_1\nu}{D\hat{u}} + \frac{a_2\nu^2}{D^2\hat{u}^2}]\frac{\hat{u}^2}{D} + \frac{g\beta}{L}\int(\hat{T} - T_1)d\hat{s} = -\frac{\Delta P}{\rho_1 L} + g \,. \qquad [7]$$

At steady state and assuming uniform heat flux, equation [7] becomes,

$$+/-[a_o + \frac{a_1\nu}{D\hat{u}} + \frac{a_2\nu^2}{D^2\hat{u}^2}]\frac{\hat{u}^2}{D} + \frac{g\beta q''P_h}{\hat{u}\rho C_p A} = -\frac{\Delta P}{\rho_1 L} + g \,. \qquad [8]$$

The plus and minus signs in front of the friction term in equation [8] are associated with the downflow and upflow directions, respectively. A plot of equation [8] (Figure 6) for typical experimental conditions in the outer channel shows that for downflow, there are possibly two solutions for $\hat{u}$ for the same imposed ΔP. A third solution is also possible in the case of upflow. Conditions for which multiple solutions, i.e., instability, occur can be determined by linear stability analysis, as developed below:

Nondimensionalize equation [7] using

$$T = \frac{\hat{T} - T_1}{\Delta Ts} \qquad u = \frac{\hat{u}}{Us}$$

$$s = \frac{\hat{s}}{L} \qquad t = \frac{\hat{t}}{L/Us}$$

where ΔTs - steady state channel temperature rise

Us - steady state channel velocity .

Dividing the left hand side by the right hand side in equation [7] , the nondimensional momentum equation is then,

$$I\frac{du}{dt} + A_0u^2 + A_1u + A_2 + (B_0 + B_1)\int Tds = 1 \qquad [9]$$

where $$I = (Us^2/L)/(-\frac{\Delta P}{\rho_1 L} + g))$$

$$A_0 = (Us^2\frac{a_0}{2D})/(-\frac{\Delta P}{\rho_1 L} + g)$$

$$A_1 = (Us\frac{a_1\nu}{2D^2})/(-\frac{\Delta P}{\rho_1 L} + g)$$

$$A_2 = (\frac{a_2\nu^2}{2D^3})/(-\frac{\Delta P}{\rho_1 L} + g)$$

$$B_0 = (g\beta\Delta Ts)/(-\frac{\Delta P}{\rho_1 L} + g))$$

$$B_1 = -(\frac{a_1\alpha\nu}{2D^2})/(-\frac{\Delta P}{\rho_1 L} + g)\,. \qquad [10]$$

The energy equation is

$$\frac{\partial\hat{T}}{\partial\hat{t}} + u\frac{\partial\hat{T}}{\partial\hat{s}} = \frac{q'' P_h}{\rho_1 C_p A}\,. \qquad [11]$$

The nondimensional energy equation becomes

$$\frac{\partial T}{\partial t} + u\frac{\partial T}{\partial s} = 1\,. \qquad [12]$$

We linearize the nonlinear differential equations by assuming small perturbations about a steady state,

$$T = Ts + T' \qquad u = u_s + u'\,. \qquad [13]$$

The linearized energy equation after subtracting the steady state terms becomes,

$$\frac{\partial T}{\partial t} + u'\frac{\partial T}{\partial s} + u_s\frac{\partial T'}{\partial s} = 0\,. \qquad [14]$$

Assume solutions of the form:

$$u' = \tilde{u}\,e^{\omega^* t} \qquad T' = \tilde{T}e^{\omega^* t}\,, \qquad [15]$$

where ω^* is the growth rate, and in general is a complex number.

The nondimensional energy equation can then be rewritten,

$$\frac{\partial T}{\partial s} + \omega^* T + u = 0 , \qquad [16]$$

where we use the fact that $u_s = 1$.

Integrating the above equation between channel inlet to channel outlet and using the boundary condition, $T = 0$ at $s = 0$,

$$T = \frac{u}{\omega}(e^{-\omega s} - 1) . \qquad [17]$$

Inserting equation [17] into equation [9] and integrating from the inlet to the outlet of the channel gives the characteristic equation,

$$I\omega^2 + 2A_0 + A_1 + \frac{B_0 + B_1}{\omega}(1 - e^{-\omega} - \omega) = 0 . \qquad [18]$$

Roots of the characteristic equation which are positive lead to an exponentially growing disturbance and an unstable situation. For marginal stability, the Mikailov criterion (5) may be used, where ω is set to $i\omega$, and the real and imaginary parts of equation [18] are set to zero. It is thus found that $\omega << 1$, implying long time constants as confirmed in the experiment. Thus, the exponential factor, $e^{-\omega}$, may be expanded in a Taylor series where the first three terms are sufficient. This leads to:

$$\omega = \frac{1}{I}[\frac{(B_0+B_1)}{2} - (2A_0 + A_1)] . \qquad [19]$$

For stability, ω must be negative, which leads to the criterion,

$$\frac{(B_0+B_1)}{2} < 2A_0 + A_1 . \qquad [20]$$

In control theory (5), the exponential factor in equation [18] is associated with a time delay. Physically in the experiment, a disturbance that reduces the flow leads to increased heating of the fluid and increases the bouyancy. This further reduces the flow and amplifies the

disturbance, although with an inertial lag. When the phase shift of the heating effect with respect to the disturbance reaches a critical value, instability results.

The data for initial flow instability (Figure 5) is replotted in Figure 7 using the parameters of equation [20]. Here, the actual measured fluid temperature rises and the outer channel flows measured under unheated conditions are used. The data appear to be relatively well correlated by equation [20] .

The criterion equation [18] can be recast using dimensionless numbers. Dividing the left hand side of [18] by the right hand side gives the ratio, $\frac{Gr}{Re^{2}*f}$. This is a ratio of the bouyancy force per unit volume to the inertia force per unit volume multiplied by friction factor. At low flows, the bouyancy force becomes significant relative to the inertia force. We see then that at low flows, this ratio is a more realistic criterion than Stanton number which is used for correlation of flow instability at high flows.

Equation 18 provides an explanation for the initiation of flow instability at the outer channel. Among the three channels, the outer channel has the highest power-to-flow ratio, and from equation [18], the bouyancy term, B_0 factor which is conducive to instability, is proportional to temperature rise. The middle channel has the largest hydraulic diameter, which from the friction term, tends to instability. However, the net effect is that the outer channel reaches instability first.

DISCUSSION

At the low flows of the experiment, natural convection forces are important and lead to complex modes of flow instability and flow reversal within the parallel channel system of the SRS fuel assembly. In contrast to the case of high flow, the system behavior at low flow is not controlled by local heat flux effects. The flow instability data for these tests did not correlate with the Stanton number which has been successfully used with flow instability data at high flows. This is to be expected because at high flows, the inertia force is much greater than the bouyancy force; consequently, flow instability is caused by changes in the system pressure drop characteristic curve as a result of boiling in the channel. Stanton number, being related to the heat transfer at the heated wall, indicates the point of incipient boiling. On the other hand, the flow instability analysis presented here demonstrate that the dimensionless group $(N_{Gr}/(N_{Re}{}^2 f)$ provide a good correlation with the low flow data, implying that the bouyancy force is of the same order of maginitude as the inertia force. The bouyancy induced flow instability initiated boiling at the heater wall.

Initiation of flow instability and flow reversal locally in a subchannel or channel did not result in rapid propagation of instability throughout the assembly mockup. Because of the high thermal conductivity of aluminum, heat could be removed by conduction to adjacent subchannels or channels; thus, there was a gradual increase in the number of outer subchannels exhibiting flow reversals with increasing power. This probably caused a flow reduction in the outer channel and redistribution to the middle and inner channels. A dryout occurred at the upper region of the outer heater when the flows in the outer and middle channels surrounding the outer heater were reduced.

CONCLUSIONS

Tests were performed on a full scale prototypic mockup of a SRS fuel assembly at low flow and low power conditions representing a loss-of-pumping accident. The results indicate that flow instability is initiated at assembly powers much less than those required for incipient boiling in the channels. The mode of instability is that of initial flow fluctuations and subchannel flow redistribution, followed by progressive subchannel flow reversals and localized boiling, progressive channel reversal, and finally dryout in one channel. A large margin exists between the point of initial flow instability, and the point of dryout and thermal excursion.

NOTATION

a_0, a_1, a_2	constants in equation [6]
A_0, A_1, A_2	defined by equation [10]
A	channel cross-sectional area
B_0, B_1	defined equation [10]
C_p	specific heat of fluid
f	friction factor
g	acceleration due to gravity
Gr	Grashof number
I	defined by equation [10]
L	channel length
P_h	heated perimeter
ΔPi	channel pressure drop
ΔPn	sytem pressure drop
q"	channel wall heat flux
R	ratio of assembly power to power required to reach bulk fluid saturation at the channel exit
Re	Reynolds number
$\hat{s}$, s	dimensional and nondimensional length in channel direction
$\hat{T}$, T	dimensional and nondimensional fluid temperature
T1	inlet temperature
T'	nondimensional temperature perturbation
$\widetilde{T}$	amplitude of temperature perturbation
Ts	steady state temperature

Tsat	saturation temperature
Twall	maximum heater wall temperature
ΔTs	channel temperature rise for heat flux q"
$\hat{u}$, u	dimensional and nondimensional velocity
u'	nondimensional velocity perturbation
$\tilde{u}$	amplitude of velocity perturbation
Us	channel velocity for heat flux q"

Greek

α	coefficient of fluid viscosity variation with temperature
β	coefficient of fluid density variation with temperature
ρ	fluid density
ν	fluid viscosity
ω^*, ω	dimensional and nondimensional propagation rate
ω	modulus of ω
∂	partial derivative operator
$\int$	integration sign

REFERENCES

1. Fighetti, G., et. al., "Flow Instability in a Vertical Annulus Under Steady State and Transient Conditions," AICHE Symposium Series 288, Vol. 88, 1992, pp. 98-105.

2. Zhou, K. and H. H. Bau, "On the Stability and Flow Reversal of Pressure Driven Flow

in an Asymmetrically Heated U-Shaped Tube, Journal of Heat Tranfer, Vol. 107, February, 1985, pp. 112 - 117.

3. Chato, J. C., "Natural Convection Flows in Parallel Channel Systems," Journal of Heat Transfer, November 1963, pp. 339-345.

4. Takeda, T. H. Kawamura, and M, Seki, " Natural Circulation in Parallel Vertical Channels with Different Heat Inputs, " Nuclear Enginering and Design, Vol. 104, 1987, pp. 133-143.

5. E.P. Popov, The Dynamics of Automatic Control Systems, Pergamon Press, 1962.

ACKNOWLEDGMENT

The information contained in this article was developed during the course of work under Contract No. DE-AC09-89SR18035 with the Department of Energy.

Table 1
Assembly Mockup Power to Reach Various Criterions

Test Point	Flow	Tin		Criterion	Power (kw)	
	kg/sec	℃	First instability	Flow reversal	Twall=Tsat	Thermal excursion
SP-IV-3	294	25.2	183.2	197	197	231.4
SP-IV-4	196	25.1	106.8	106.8	129.8	160.6
SP-IV-5	98	25.2	36.1	36.1	75.5	90.3
SP-IV-6	294	40.5	132	161	161	188.2
SP-IV-7	196	40	74	87.7	93.8	131.5
SP-IV-8	98	40.9	19.4	19.4	53.5	74.2
SP-IV-6R	294	403	160.2	172	172	188
SP-IV-4R	196	25.1	105.8	105.8	129.6	160.8
SP-IV-8R	98	40.8	56.5	56.5	60.7	74.7

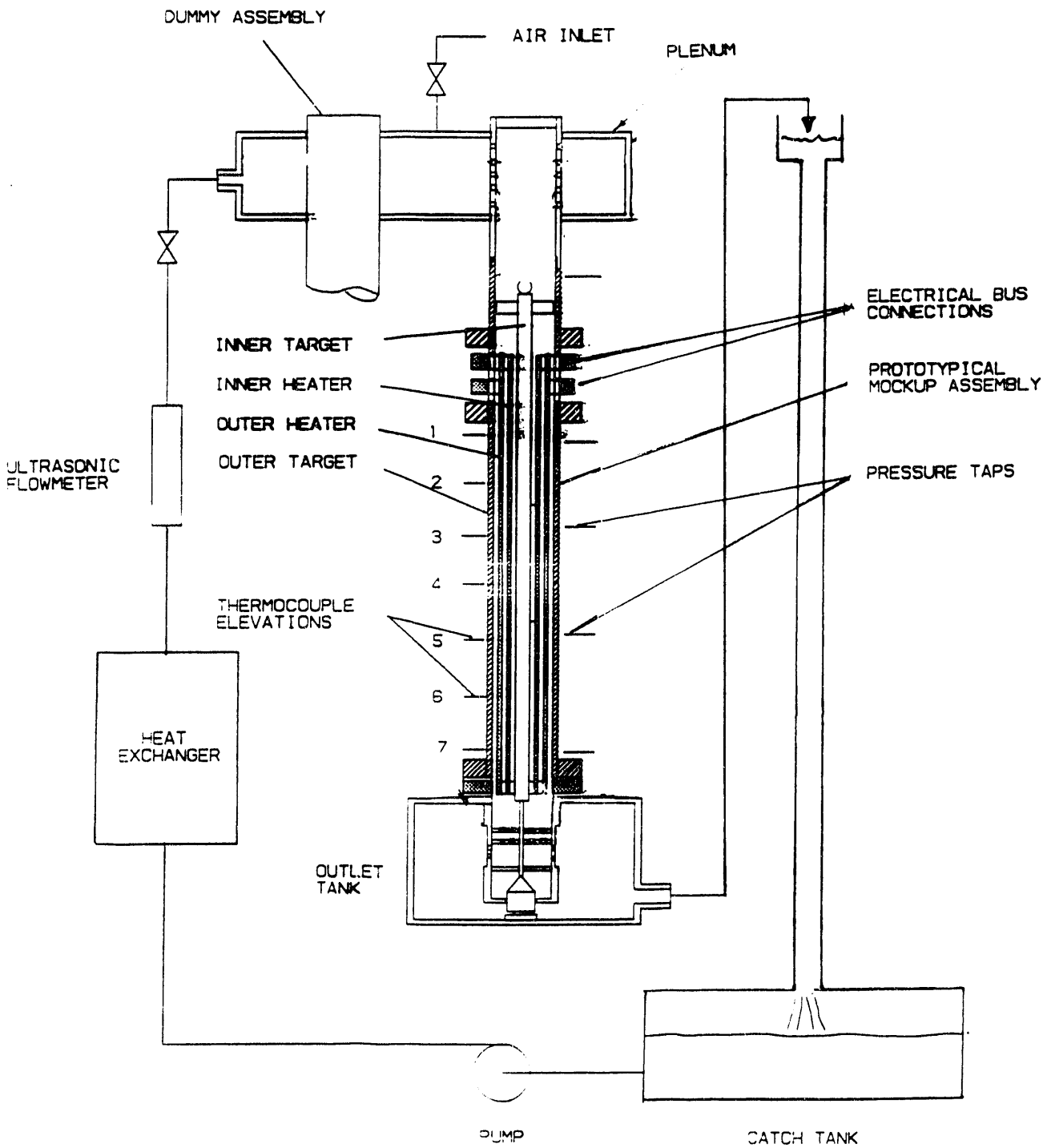

Figure 1 Test Assembly Mockup and Test Loop

Figure 2 Cross-sections of SRS Fuel Assembly Mockup

and Prototypic Heaters

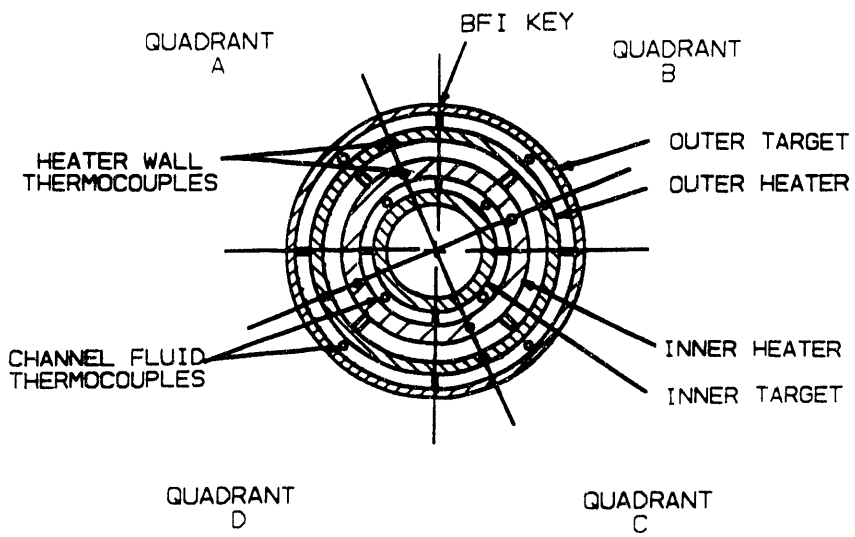

a) SRS Fuel Assembly Mockup

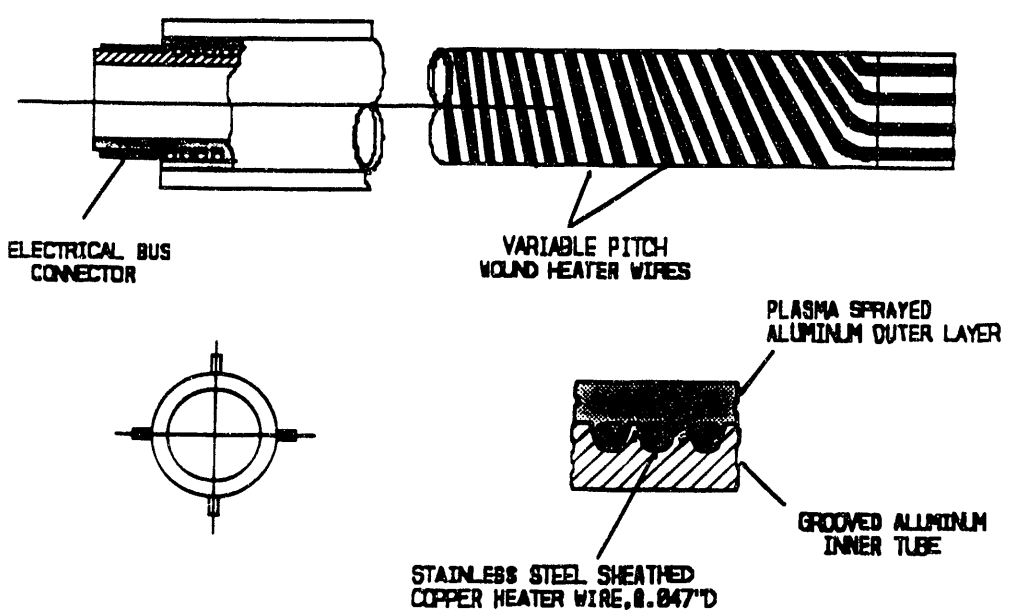

(b) Prototypic heater design

Figure 3a Temperature Profiles for Stable Flow

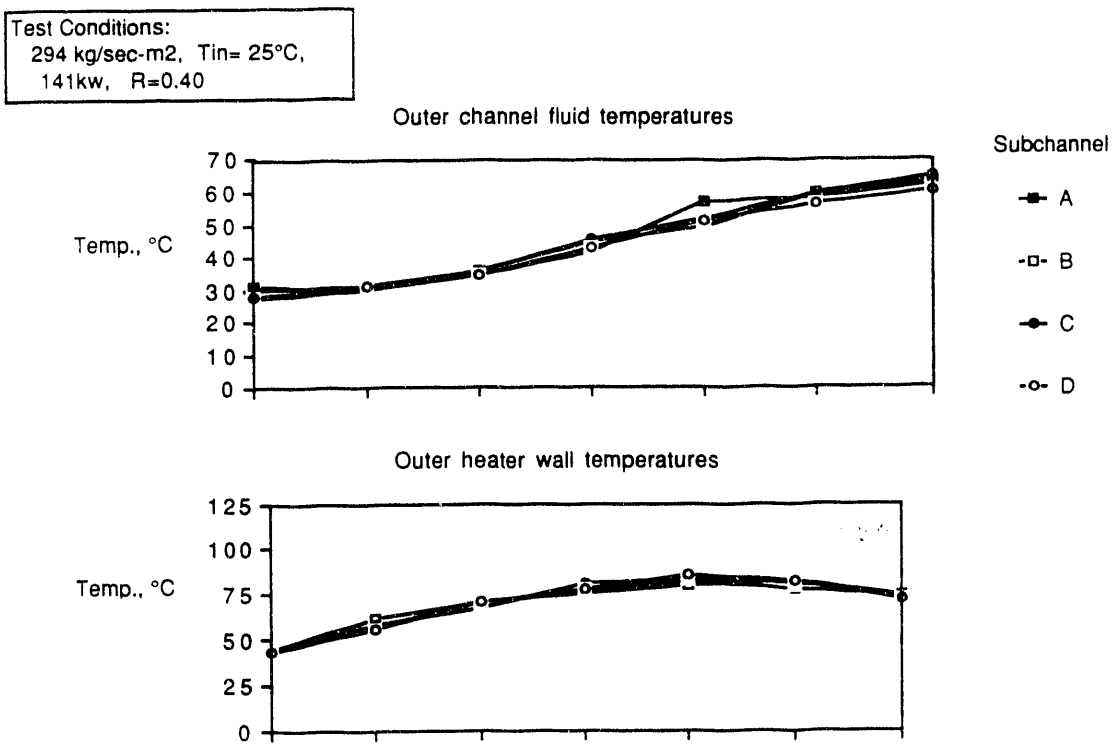

Figure 3b Temperature Profiles for Unstable Flow

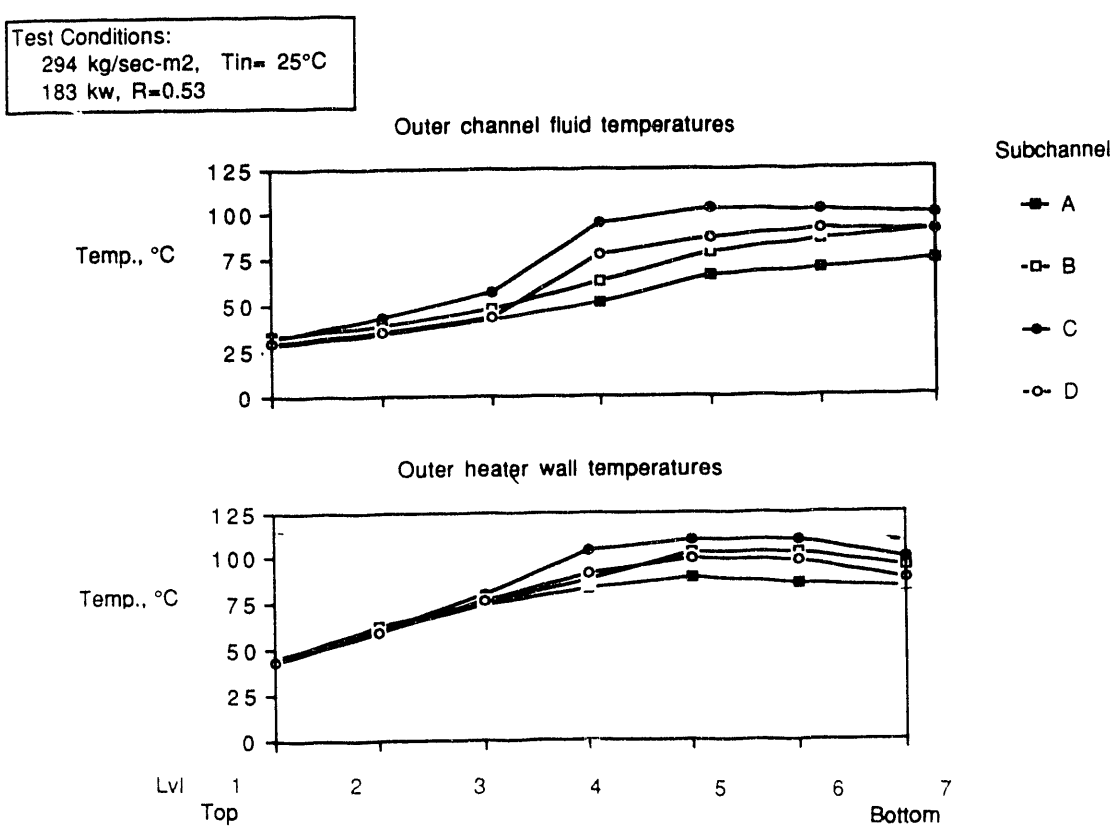

Figure 3c Temperature Profiles with Local Flow Reversal and Wall Temperature at Saturation

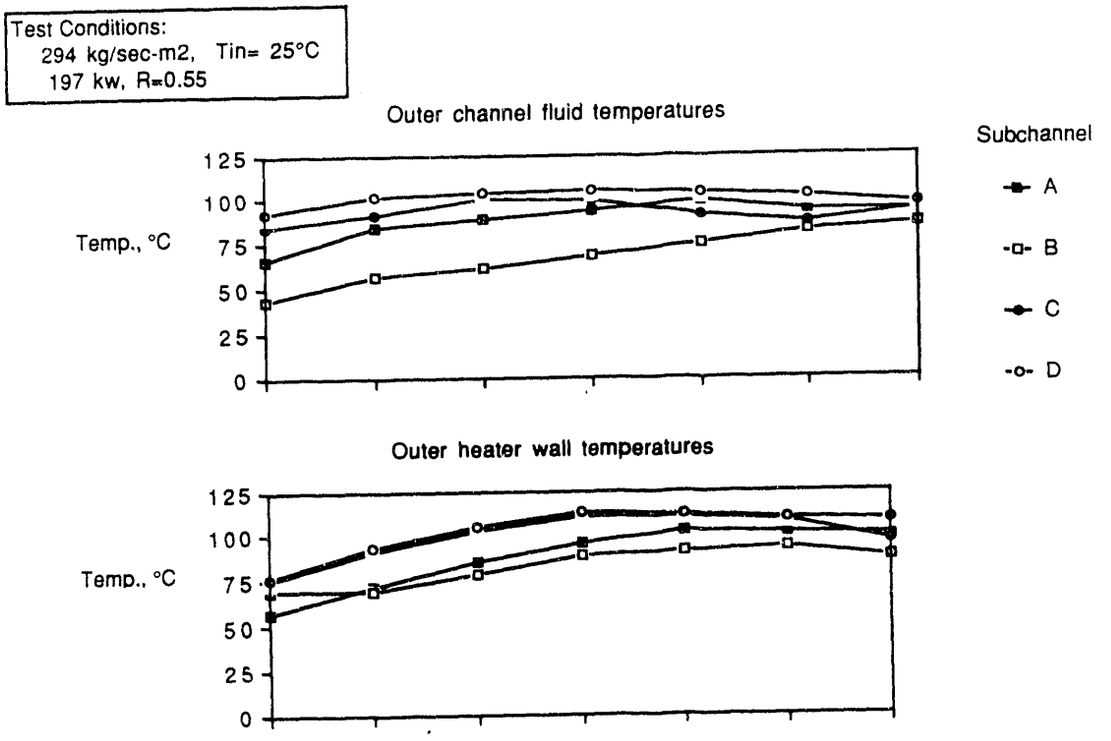

Figure 3d Temperature Profile with Full Flow Reversal in Outer Channel Prior to Thermal Excursion

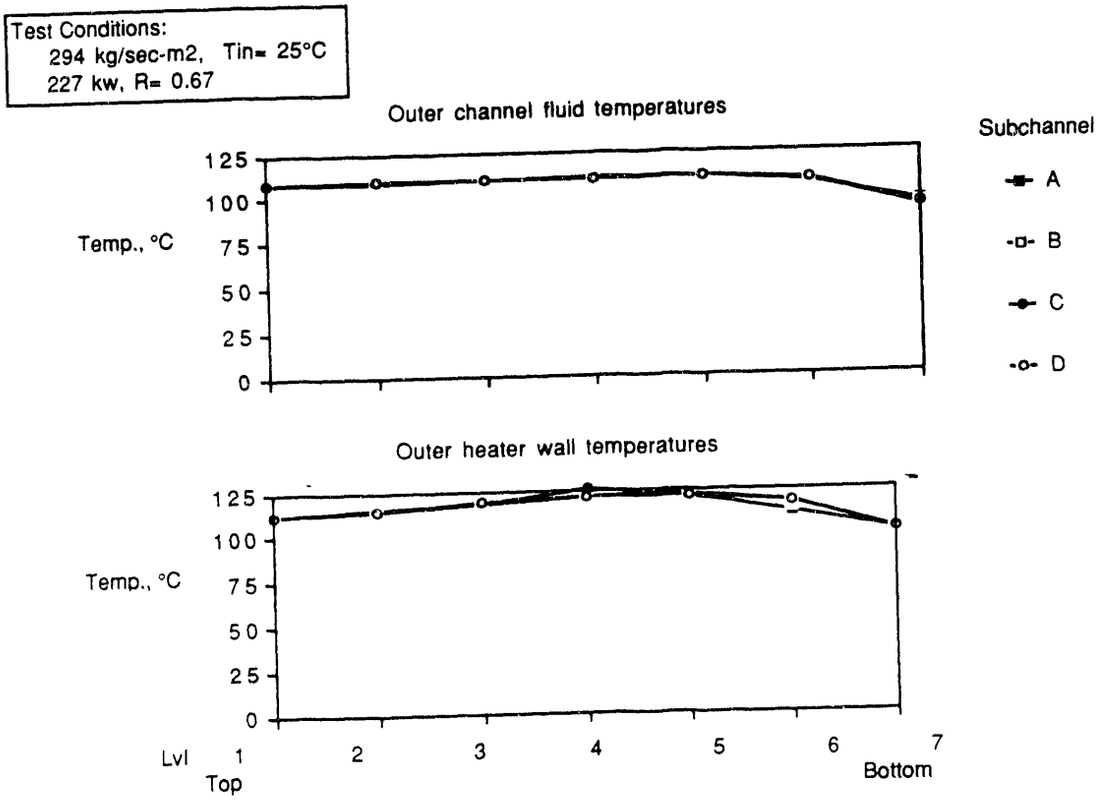

Figure 4 Fluid Temperature Fluctuations at Initial Point of Instability

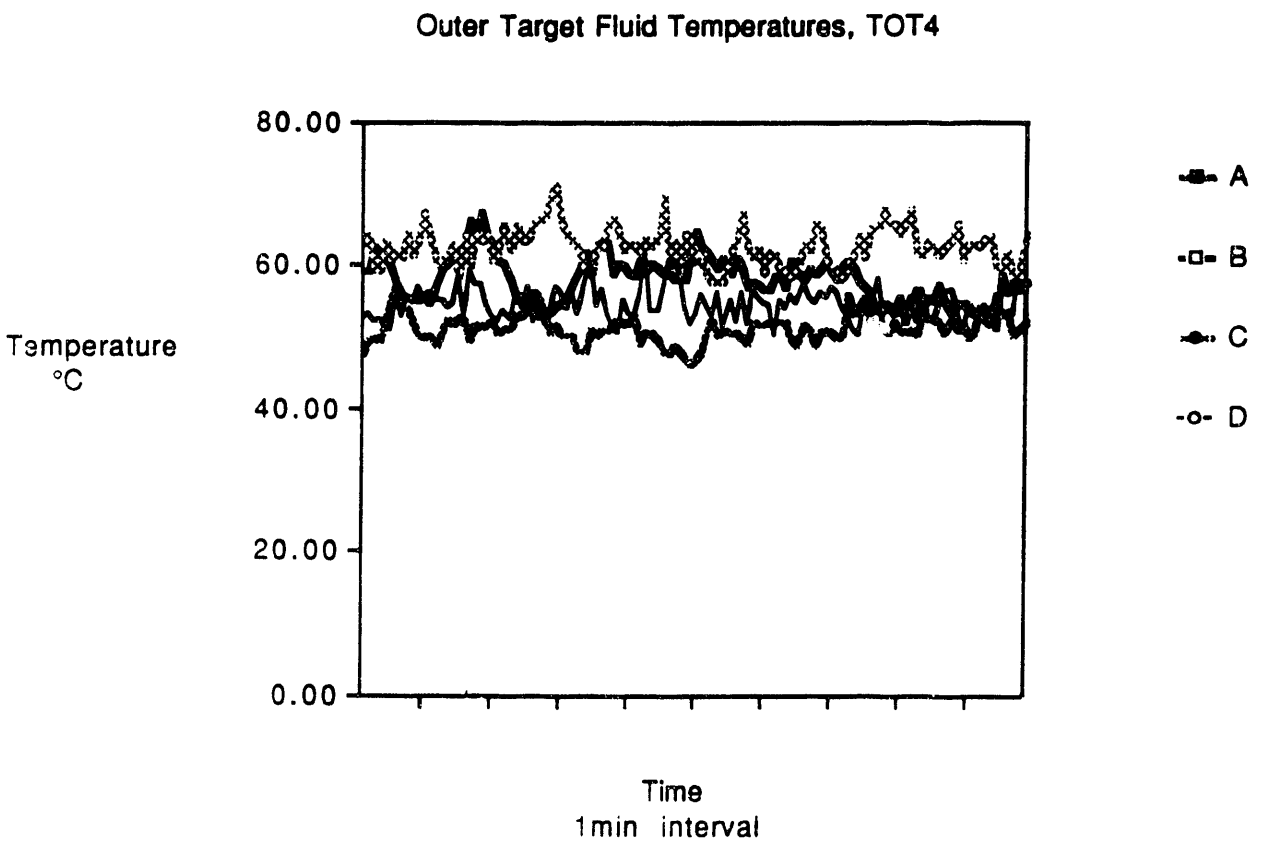

Figure 5 Plot of Assembly Mockup Power
at Various Flow Instability Stages

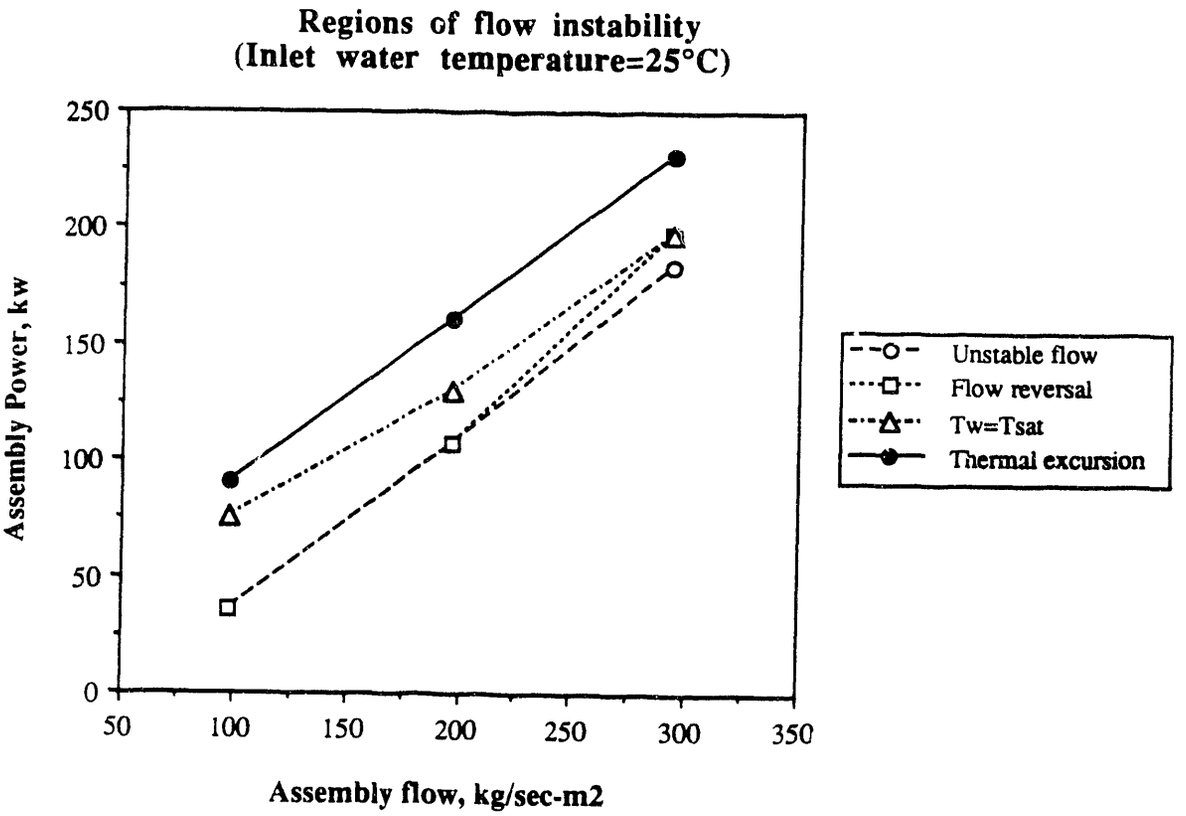

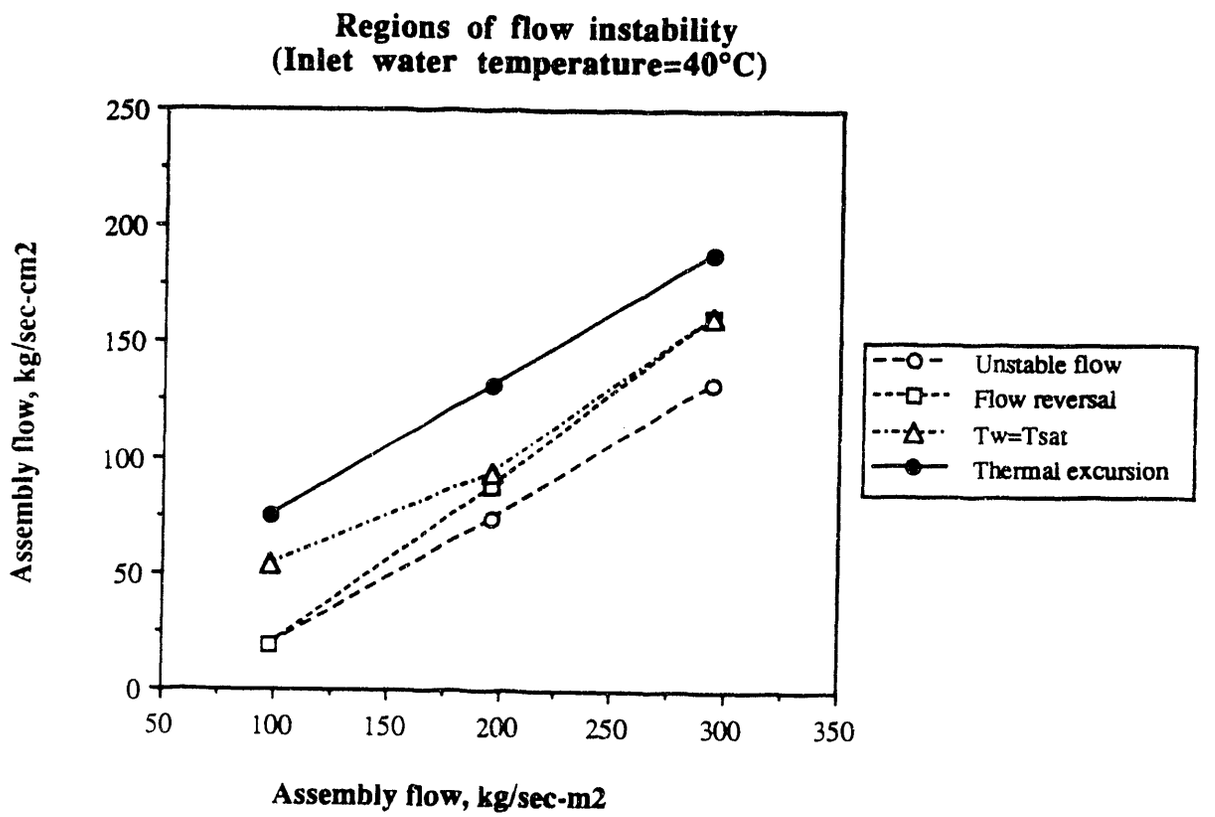

Figure 6 Balance of Forces at Steady State

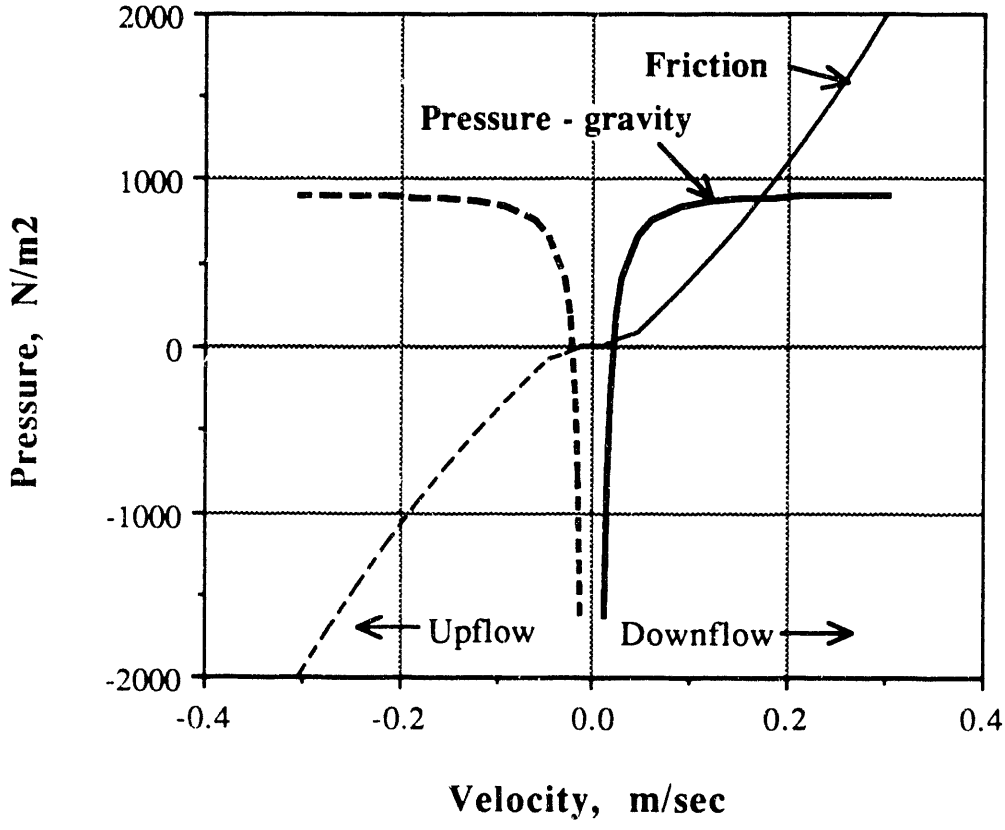

Figure 7 Correlation of Experimental Data
by Linear Stability Analysis